Palaeogeography, Palaeoclimatology, Palaeoecology 600 (2022) 111064

Contents lists available at ScienceDirect

Palaeogeography, Palaeoclimatology, Palaeoecology

journal homepage: www.elsevier.com/locate/palaeo

The Eocene-Oligocene climate transition in the Alpine foreland basin: Paleoenvironmental change recorded in submarine fans

Euan L. Soutter [a,*], Ian A. Kane [a], Ander Martínez-Doñate [a], Adrian J. Boyce [b], Jack Stacey [a], Sébastien Castelltort [c]

[a] Department of Earth and Environmental Sciences, University of Manchester, Manchester, UK
[b] Scottish Universities Environmental Research Centre, East Kilbride, UK
[c] Department of Earth Sciences, University of Geneva, Geneva, Switzerland.

ARTICLE INFO

Editor: Dr. Paul Hesse

Keywords:
Paleoclimate
Submarine fans
Stratigraphy
Sea-level
Alps
Foreland basin

ABSTRACT

The Eocene-Oligocene transition (EOT) was a period of considerable environmental change, signifying the transition from Paleocene greenhouse to Oligocene icehouse conditions. Preservation of the sedimentary signal of such an environmental change is most likely in net-depositional environments, such as submarine fans, which are the terminal parts of sedimentary systems. Here, using sedimentary and stable isotope data from the Alpine foreland basin, we assess whether this major climatic transition influenced the stratigraphic evolution of submarine fans. Results indicate that fine-grained deposition in deep-water environments corresponds to positive $\delta^{13}C$ excursions and eustatic highstands, while coarse-grained deposition corresponds to negative $\delta^{13}C$ excursions and eustatic lowstands during the earliest Oligocene. While alternative explanations cannot be ruled out on the basis of this dataset alone, our results suggest that eustatic fluctuations across the EOT and into the early Oligocene influenced sediment supply to deep-water environments.

1. Introduction

The stratigraphic record of major environmental change is expected to be best recorded in net-depositional environments, such as submarine fans (e.g. Hessler and Fildani, 2019). Submarine fans are built from the deposits of sediment-gravity flows that transport vast quantities of terrigenous sediment and organic carbon to deep-marine environments (e.g. Galy et al., 2007). Submarine fan growth has been shown to occur during both low and high eustatic sea levels (e.g. Covault et al., 2011) and may be driven by a combination of tectonic events (e.g. Howarth et al., 2021) and onshore climate change (e.g. Picot et al., 2019), all of which can be overprinted by autogenic processes. Disentangling allogenic from autogenic influences on submarine fan deposition has therefore proven to be difficult (Ferguson et al., 2020), with allogenic signals often attenuated within the sediment routing system (Romans et al., 2016). Measurement of $\delta^{13}C$ in exhumed stratigraphy has been used as a means of addressing this problem, with $\delta^{13}C$ sensitive to many of the environmental factors that influence submarine fan deposition (e.g. Castelltort et al., 2017). Positive $\delta^{13}C$ excursions are considered to correspond to high sea-levels, flooded continental shelves, high biological productivity and burial of ^{12}C, while low $\delta^{13}C$ values correspond to low-sea levels, exposed shelves, lower productivity and greater run-off (Jenkyns, 1996; Castelltort et al., 2017). By constructing a $\delta^{13}C$ curve through a deep-marine sequence of a known age it is therefore possible to relate sedimentation to eustatic and climatic trends (Castelltort et al., 2017).

The Eocene-Oligocene climate transition (EOT) between ~34 and ~33 Ma was a major environmental response to the opening of oceanic gateways in the Southern Oceans (Kennett, 1977), decreased atmospheric CO_2 (Pearson et al., 2009) and orbital forcing (Ladant et al., 2014), and resulted in the establishment of major Antarctic ice sheets (Liu et al., 2009), and the transition from Paleogene greenhouse to current icehouse conditions (Wade et al., 2012). The EOT occurred through a series of global cooling 'steps' that correspond to positive $\delta^{18}O$ excursions and faunal extinctions around the Eocene-Oligocene boundary (EOB), such as the 'Oi-1' event at ~33.55 ma, which represents a major eustatic sea-level fall related to Antarctic ice sheet growth (Katz et al., 2008). In an attempt to standardise terminology and correlation, the 'Oi-1' event has since been termed the 'Earliest Oligocene Oxygen Isotope step' (EOIS), along with other isotopic events between

* Corresponding author.
E-mail address: euan.soutter@manchester.ac.uk (E.L. Soutter).

https://doi.org/10.1016/j.palaeo.2022.111064
Received 2 November 2021; Received in revised form 17 May 2022; Accepted 17 May 2022
Available online 20 May 2022

the late Eocene and early Oligocene, such as the 'Priabonian oxygen isotope maximum' (PrOm) and the 'Early Oligocene Glacial Maximum' (EOGM), which is bound at the base by the EOIS (Hutchinson et al., 2021).

Environmental change related to these events has been recorded in Eocene and Oligocene sediments, with shallow marine erosion surfaces in Alabama (Miller et al., 2008) and deposition of calcareous turbidites adjacent to Pacific atolls (Schlanger and Premoli Silva, 1986) correlated to early Oligocene $\delta^{18}O$ excursions and associated cooling and sea-level fall. In terrestrial environments, long-term cooling during the EOT drove global changes in flora, fauna and the hydrological cycle (Hutchinson et al., 2021), with increased aridity identified in sediments from Texas (Yancey et al., 2003) to Tibet (Page et al., 2019), and increased seasonality inferred from pollen and spore assemblages across the northern high latitudes (Eldrett et al., 2009). These trends are complex on a global scale, however, with changes in the hydrological cycle across the EOT sometimes difficult to disentangle from regional tectonic forcings (Chamberlain et al., 2012), and little evidence for terrestrial cooling and aridity present at all in certain regions (Hutchinson et al., 2021).

The Grès d'Annot Formation is an exhumed siliciclastic deep-marine succession that was deposited within the Alpine foreland basin during the EOT and the EOGM (Fig. 1A, B; Fig. 2) (Joseph and Lomas, 2004). The Grès d'Annot records a common deep-marine stratigraphic pattern of fine-grained intervals interspersed with coarser-grained intervals, with each >10 m thick interval composed of numerous individual event beds. This apparent cyclicity has been attributed to sea-level change and tectonism (Fig. 2) (Callec, 2004; Euzen et al., 2004); however, the relative impact of these controls has not been tested. This study therefore aims to investigate, through high-resolution isotopic analysis of the Grès d'Annot stratigraphy, whether: 1) the EOT and associated eustatic and climatic change in the early Oligocene is resolved in the Grès d'Annot isotopic record, and 2) whether this environmental change affected submarine fan deposition in the Alpine foreland basin. On a broader scale, this study aims to explore how the isotopic records of exhumed submarine fans can be used to understand how past landscapes responded to environmental change.

2. Study area: Chalufy

One of the most well-studied Grès d'Annot exposures is located at the Montagne de Chalufy (Fig. 1A; B), representing a relatively distal part of the Grès d'Annot submarine fan system (Du Fornel et al., 2004) (Fig. 1A; Fig. 2B). The exposure comprises three coarse-grained sandstone intervals deposited sequentially against a marl paleo-slope (Puigdefàbregas et al., 2004) (Fig. S1). The coarse-grained intervals are interpreted as the deposits of high-concentration turbidity currents that built submarine fan lobes on the basin floor. These coarse-grained intervals alternate with finer-grained mudstone and siltstone intervals, which are interpreted as the deposits of lower-concentration turbidity currents, interbedded with thin hemipelagic mudstones deposited at the distal extents of the coarse-grained lobes or distributary channels on the basin floor (Fig. 2; Fig. S1).

Identification of foraminifera belonging to known planktonic (P18) and nano-planktonic (NP21) biozones within the Chalufy section indicates that the basal part of the section was deposited at a maximum of ~33.8 Ma (base P18), with the uppermost parts of the Grès d'Annot being deposited at a minimum of ~32 Ma (top P18) (Fig. 2A) (Euzen et al., 2004; Du Fornel et al., 2004). The entire section therefore spans a maximum of ~1.8 myr, with the boundaries between each coarse-grained interval presently unconstrained chronologically. Constraining the timing of these coarse-grained intervals was therefore an aim of this study. For consistency with the existing Alpine foreland chronostratigraphic framework, and other isotopic and eustatic datasets used, all ages are tied to the chronology of Berggren et al. (1995).

3. Data and methods

105 samples were recovered from three fine-grained intervals in one continuous measured section (~148 m) spanning the Grès d'Annot exposure at the Chalufy paleo-slope (Fig. 3; Fig. 2, S1; S2; Table S1). The samples were collected at ~60 cm intervals, from >30 cm below the exposed surface and only within sections interpreted as being deposited by hemipelagic settling, in order to avoid potential contamination by allochthonous material deposited by turbidity currents. The potential presence of microscopic turbidites not visible at outcrop is unavoidable (e.g. Boulesteix et al., 2019), however a high-sampling density was designed to mitigate against this as much as possible. The samples were crushed and their bulk carbonate $\delta^{13}C$ and $\delta^{18}O$ values measured using standard techniques (Brodie et al., 2018), with 17 repeated measurements of section-representative samples yielding a mean measurement error of ±0.3 for $\delta^{13}C$ and ± 0.1 for $\delta^{18}O$ (Fig. 3; S2). Carbon and oxygen isotopes are reported per mil (‰) relative to the Vienna Pee Dee Belemnite Standard (VPDB) (Fig. S2).

Three isotopic curves representing each fine-grained interval were generated through the application of a Savitzky–Golay filter to the individual data points, which smooths the data without distorting the underlying signal (Fig. 3; S2; S3) (Savitzky and Golay Savitzky and Golay, 1964). The data were iteratively smoothed through various window-lengths until a dominant signal emerged (Fig. S7). These curves were then placed within bounding-age constraints derived from

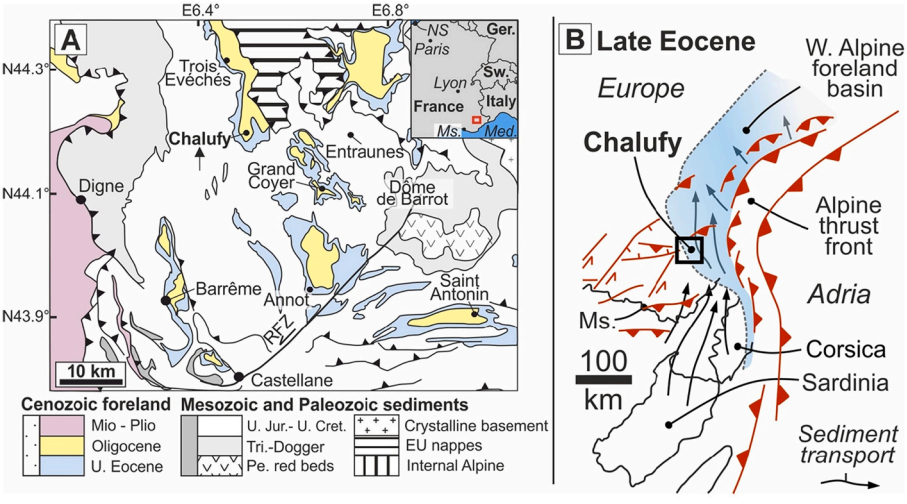

Fig. 1. A) Geological map of the Alpine foreland and the location of the sampled section at Montagne de Chalufy (black arrow). Inset is present-day European location. Red box is geological map area. Black lines with teeth represent thrust faults, with teeth on hangingwall. (modified from Joseph and Lomas, 2004). U. = upper; Mio-Plio = Miocene-Pliocene; Jur. = Jurassic; Cret. = Cretaceous, Tri. = Triassic; Pe = Permian. EU = Embrunais-Ubaye. B) Palinspastic reconstruction and paleogeographic setting of the Alpine foreland basin during the Late Eocene (modified from Dumont et al., 2011). The approximate location of Chalufy is indicated. Ms. = Marseille; NS = North Sea; Sw. = Switzerland; Ger. = Germany; Med. = Mediterranean. (For interpretation of the references to colour in this figure legend, the reader is referred to the web version of this article.)

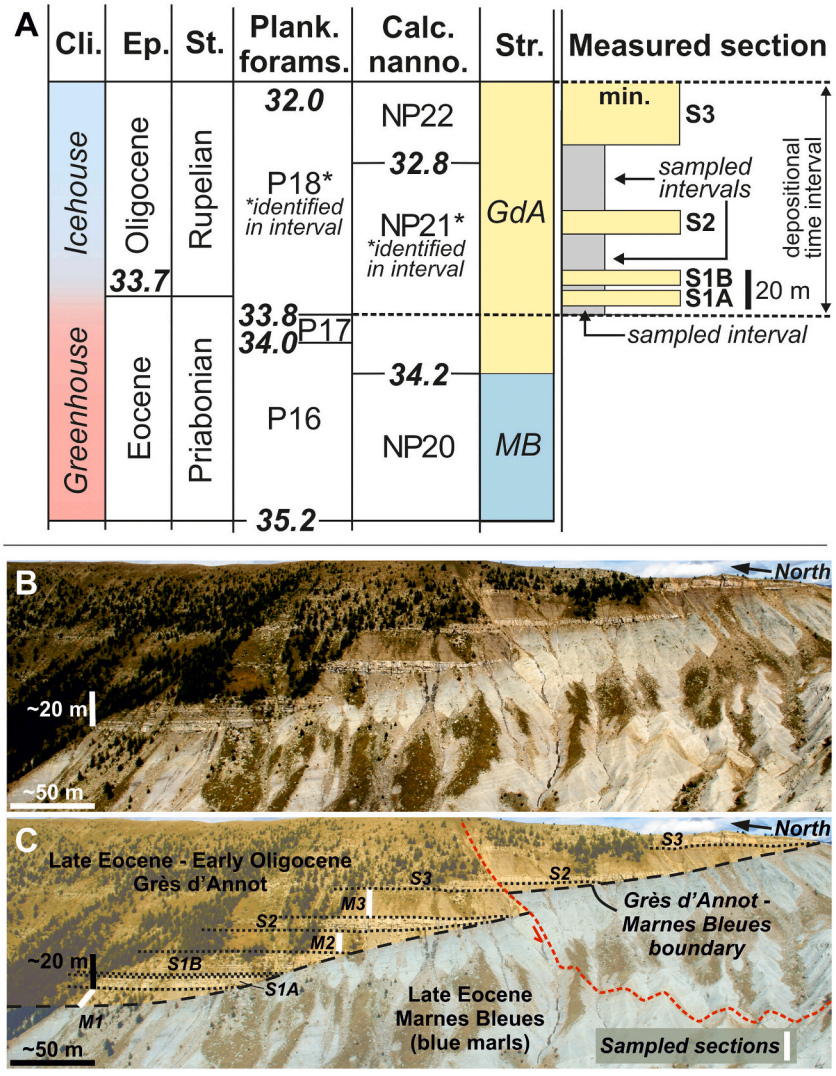

Fig. 2. A) Chronostratigraphic framework of the studied section (modified from Euzen et al., 2004). Micropaleontological zonation (NP & P zones) of the studied stratigraphy (modified from Euzen et al., 2004). Eocene – Oligocene boundary shifted to that of Katz et al. (2008). B) Uninterpreted and interpreted (C) sampled sections at Chalufy and stratigraphic context. Red dashed line indicates a fault. Grid reference: 44°09′21"N, 6°32′51E. GdA = Gres d'Annot; MB = Marnes Bleues; Cli. = generalized climate; Ep. = epoch; St. = stage, Plank. forams = planktonic foraminifera; Calc. nano. = calcareous nannofossils; Strat: stratigraphy; P: planktonic; NP: nanoplanktonic; S = sandstone; M = mudstone. (For interpretation of the references to colour in this figure legend, the reader is referred to the web version of this article.)

micropaleontological zonation of the study area (Du Fornel et al., 2004) and visually assessed for correlation with the time-equivalent global $\delta^{13}C$ curves (Cramer et al., 2009; Westerhold et al., 2020) and eustatic sea-level curves derived from borehole backstripping of the New Jersey margin (Miller et al., 2005) and global $\delta^{18}O$ (Miller et al., 2020). Randomly selected samples have also undergone X-ray diffraction (XRD), total organic carbon (TOC) (Table S1) and petrographic analysis (Fig. S6) in order to assess the potential for mixed-carbonate-source error or diagenetic overprinting.

4. Results

The bulk $\delta^{13}C$ content was measured from 105 samples (Fig. 3; Fig. S1). The identification of benthic foraminifera during petrographic analysis of the samples (Fig. S6) and the occurrence of dateable benthic foraminifera within the Chalufy section (Fig. 2A) indicates that the bulk $\delta^{13}C$ measurements primarily record the signature of this fauna. The observed depletion in $\delta^{18}O$ values suggests a diagenetic influence, which may have also impacted the $\delta^{13}C$ values. Cross-plotting of $\delta^{13}C$ and $\delta^{18}O$ from each interval also shows no statistically-significant trends, suggesting a lack of diagenetic overprinting (Marshall, 1991) (Fig. S5), however $\delta^{13}C$ and $\delta^{18}O$ have been shown to positively correlate with the EOT (Hutchinson et al., 2021), which may limit the effectiveness of this diagenetic test. X-ray diffraction of selected samples within each interval indicates total organic carbon (TOC) contents of <0.7% and a calcite-to-organic -matter ratio of >7:1, indicating that the likelihood of diagenetic contamination from organic carbon is low (Saltzman and Thomas, 2012).

The $\delta^{13}C$ data shows a broadly increasing spread with increasing height in the section (1σ = 0.4‰, 0.9‰, 1.0‰ for each sequential fine-grained interval) (Fig. S4), with mean $\delta^{13}C$ values being 1.2‰ more negative than time-equivalent open oceanic values (Cramer et al., 2009). Data noise and more negative $\delta^{13}C$ values are attributed to: 1) the relatively proximal position of the basin resulting in the oxidation of light organic ^{12}C delivered by rivers (Jenkyns, 1996; Voigt and Hilbrecht, 1997), and 2) microscopic turbidites or authigenic carbonates, such as micro-veins, within the hemipelagic sections creating allochthonous noise (Fig. S7; S6). These unavoidable diagenetic and environmental factors could potentially modify the isotopic values, which would preclude accurate high-resolution cyclostratigraphy (e.g. precessional trends). Lower-resolution isotopic trends (e.g. eccentric trends) are suggested to be resolved, however, as a result of the high sampling density and resultant smoothed curves.

The $\delta^{13}C$ curves of Mudstone 2 (M2) and Mudstone 3 (M3) (sandstone-bounded fine-grained intervals) each show a general trend of increasing then decreasing $\delta^{13}C$ values with increasing height (Fig. 3). Within the micropalaeontological constraints these curves could be correlated to similar excursions in the smoothed global $\delta^{13}C$ curve between 33.5 and 33.0 Ma, or between two rising then falling sections of the borehole-derived eustatic curve between 33.5 and 32.3 Ma (Fig. 4).

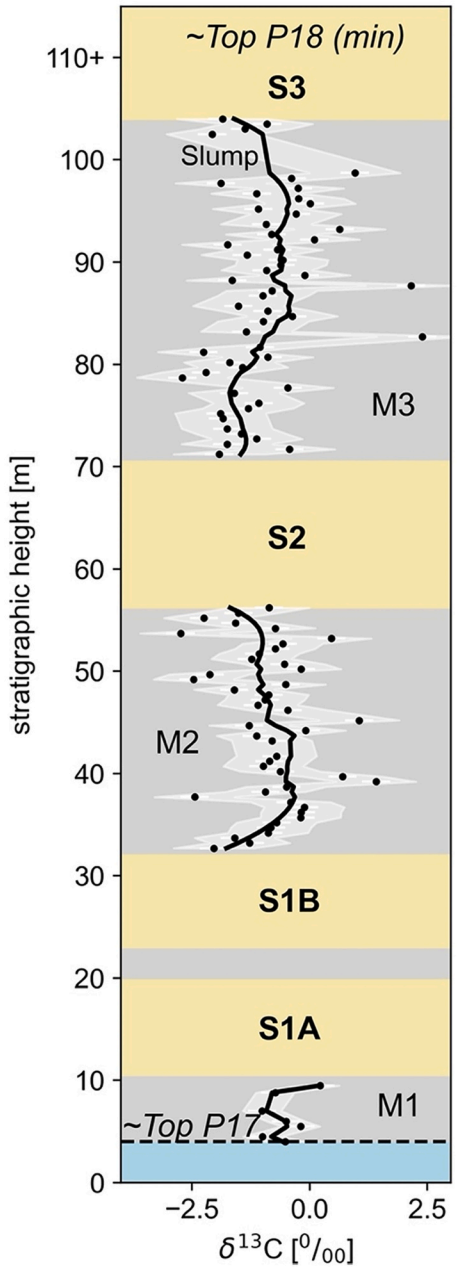

Fig. 3. $\delta^{13}C$ measurements for each fine-grained interval sampled and their bounding P-Zones (planktonic zones) (Du Fornel et al., 2004). The black solid line represents a Savitzky-Golay filter. Yellow = sandstone, grey = mudstone and siltstone, blue = marl. The white line is an uncertain age break. Error bar is the mean error of $\delta^{13}C$ repeats. Light grey envelope is one standard deviation.

Due to the restricted nature of the Alpine foreland basin (Fig. 1B), which would have prevented rapid exchange with the global carbon reservoir (Saltzman and Thomas, 2012), and the relatively proximal position of the sampled stratigraphy (Fig. 1B), the eustatic correlation is suggested to be most probable (e.g. Castelltort et al., 2017). M2 and M3 therefore correlate with eustatic sea-level highstands, with the sandstones at ends of the curves (S1B, S2 and S3) correlating with sea-level lowstands (Fig. 4).

There is uncertainty in how much time is occupied between the upper marl surface and Grès d'Annot deposition as the older part of the stratigraphy was not deposited at the sampled location, which is higher on the basin margin slope (Du Fornel et al., 2004). Accordingly, the isotopic trends within the lowermost section cannot be confidently interpreted.

The Chalufy $\delta^{18}O$ values show a generally decreasing, but noisy, trend in M2, and a sharply increasing then sharply decreasing trend in M3. However, due to diagenesis, these $\delta^{18}O$ trends are expected to be less reliable than the $\delta^{13}C$ trends and are consequently not used as a basis for interpretation (Fig. S2).

5. Discussion

5.1. Eustatic interpretation

The observed correlation between submarine fan retreat and global positive $\delta^{13}C$ excursions suggests that; 1) the isotopic record of the Chalufy section resolves cycles of environmental change across the EOIS, EOGM and the early Oligocene, and 2) deposition in the Alpine foreland was influenced by the environmental factors driving these excursions. The correlation between the positive $\delta^{13}C$ excursions and time-equivalent global eustatic highstands indicates that sea-level change drove these excursions. These sea-level highstands are not present when sea-level is reconstructed and smoothed from $\delta^{18}O$ (Miller et al., 2020), but are present when sea-level is back-stripped from boreholes (Miller et al., 2005). It may be that this highstand is the fingerprint of transient atmospheric CO_2 rise immediately after the drop in CO_2 across the EOT (Pearson et al., 2009), which is only recorded by backstripping nearer continents, and not resolved in the smoothed $\delta^{18}O$-derived curve (Fig. 4). When following this interpretation, fine-grained deposition in the deep-water foreland basin is therefore linked to high sea-levels, while coarse-grained deposition is linked to low sea-levels. These results are consistent with those made in the Eocene Pyrenean foreland basin (Castelltort et al., 2017), with positive $\delta^{13}C$ excursions found to correlate with eustatic sea-level highstands and reduced sediment supply to submarine fans.

Low sea-levels tend to enhance siliciclastic deep-marine deposition as rivers are able to deliver sediment directly to the shelf-edge and deeper waters. In the Quaternary Golo Fan this process has been invoked to explain widespread fine-grained deposition in submarine fans during interglacial highstands and coarser-grained deposition during glacial lowstands (Sweet et al., 2020). These results suggest an analogous control on sediment supply to deep-water in the Paleogene Alpine foreland basin.

Sea-level fluctuations during the early Oligocene are likely driven by fluctuations in volume of the newly-established Antarctica ice sheet (Katz et al., 2008), with the positive $\delta^{13}C$ excursions identified here likely a consequence of warmer periods with decreased ice sheet volume. This may indicate that onshore climate change across the Eocene-Oligocene transition also influenced deposition in the Alpine foreland. Warmer climates act to reduce sediment supply to submarine fans by expanding vegetation cover and trapping sediment in catchments, as observed during warm Pleistocene interglacials in the Gulf of Corinth (Cullen et al., 2021). Conversely, cooler climates may increase sediment supply to submarine fans through increased continental weathering, as invoked to explain increased terrigenous sediment supply to marine environments offshore western Africa during early Oligocene cooling (Séranne, 1999). Similar climatic mechanisms may have operated in tandem with eustasy to modulate coarse-grained sediment supply to the deep-water Alpine foreland during the early Oligocene. This may be indirectly reflected in the $\delta^{13}C$ record of the fine-grained sections, with a reduction in the volume of ^{12}C transported to marine environments by rivers consistent with the observed positive $\delta^{13}C$ excursions (Voigt and Hilbrecht, 1997).

5.2. Alternative interpretations

The inferred link between positive $\delta^{13}C$ excursions and eustatic sea-level rise appears to be dominant in the Alpine foreland basin and other foreland basins (Castelltort et al., 2017). Across the EOT and EOGM,

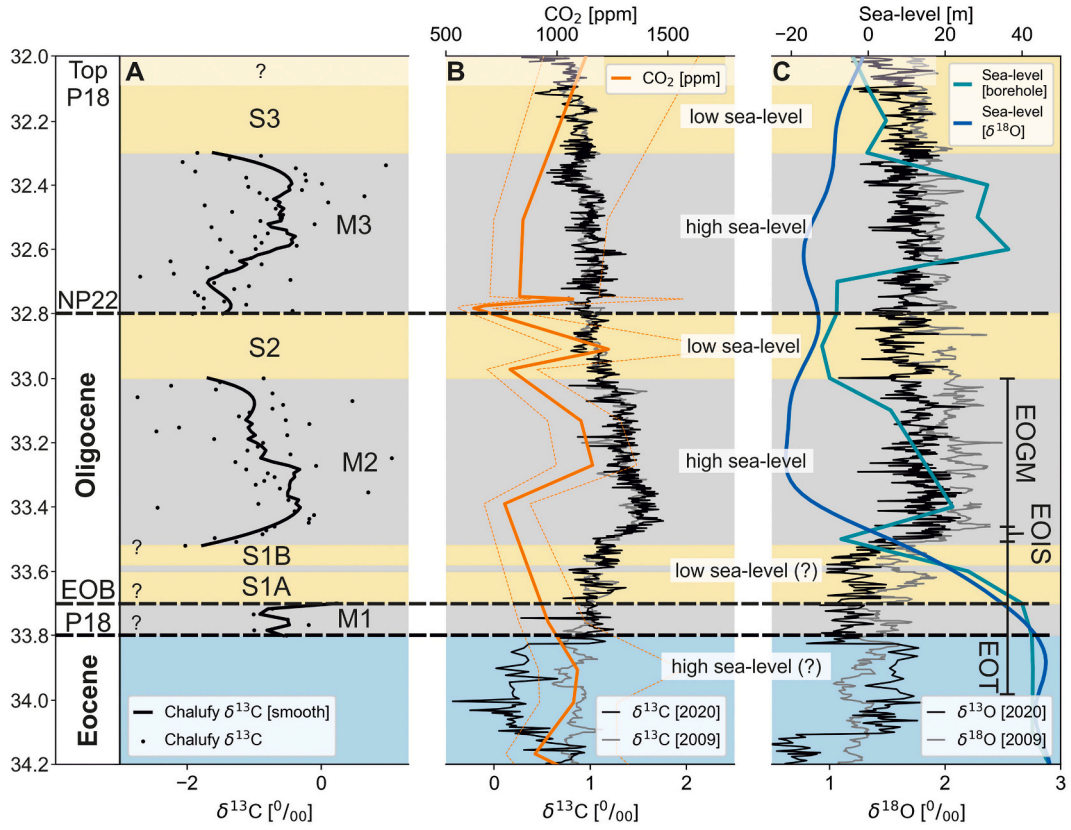

Fig. 4. Correlation of A) the $\delta^{13}C$ record from Chalufy, B) Global $\delta^{13}C$ (Cramer et al., 2009; Westerhold et al., 2020), and CO_2 curves (Beerling and Royer, 2011) C) Global $\delta^{18}O$ curves (Cramer et al., 2009; Westerhold et al., 2020), sea-level derived from borehole backstripping (Miller et al., 2005) and sea-level derived from $\delta^{18}O$ (Miller et al., 2020). C-S = Corsica-Sardinia, yellow = sandstone, grey = mudstone and siltstone, blue = marl, EOT = Eocene-Oligocene transition, EOB = Eocene-Oligocene boundary, EOIS = Earliest Oligocene oxygen isotope step, EOGM = Early Oligocene glacial maximum. Ages tied to the chronology of Berggren et al., 1995 and Cande and Kent, 1995 by tying the EOB of these studies. Solid black lines in A are Savitzky–Golay filtered data, black dots indicate raw data. (For interpretation of the references to colour in this figure legend, the reader is referred to the web version of this article.)

however, positive $\delta^{13}C$ excursions are typically attributed to cooling. Cooling may result in: 1) low sea-levels, increased weathering of relatively ^{13}C-enriched carbonate shelves and deepening of the CCD, 2) increased ocean mixing and productivity, and 3) cooling and sequestration of ^{12}C in permafrost (Armstrong McKay et al., 2016). This may indicate that reduced sediment supply to the Alpine foreland basin occurred during cooler periods associated with the EOGM, and not warm periods and highstands as the eustatic correlation would suggest. The positive $\delta^{18}O$ excursion observed within M3 may allude to this, however the $\delta^{18}O$ cannot be as confidently interpreted due to diagenesis.

Cooler climates can reduce sediment supply by enhancing aridity and reducing runoff (e.g. Leeder et al., 1998). This effect may be reflected in the $\delta^{13}C$ record of the fine-grained sections, with increased aridity reducing the quantity of ^{12}C delivered to marine environments by rivers, driving the positive $\delta^{13}C$ excursions (Voigt and Hilbrecht, 1997). Similar depositional patterns have been observed during the Quaternary, with submarine fan retreat associated with aridity in both the Congo (Picot et al., 2019) and Nile (Ducassou et al., 2009) submarine fans, irrespective of sea-level. Therefore, if the $\delta^{13}C$ record of the Alpine foreland represents the global signature, this indicates that periods of reduced deep-water sedimentation in the Alpine foreland were driven by global cooling across the EOT. This alternative interpretation is not favoured, however, because of: 1) the relatively proximal position of the sampled stratigraphic compared to the largely open-ocean samples typically used for EOT isotopic interpretations, and 2) the relatively restricted and epicontinental nature of the Alpine foreland basin (Fig. 1B; Dumont et al., 2011). These factors would likely inhibit rapid carbon exchange with the open-ocean (e.g. Saltzman and Thomas, 2012), making the proximal isotopic record more sensitive to sea-level change and associated sediment supply variation than the distal open-oceanic record. It is therefore suggested that the isotopic record of proximal Alpine foreland basin may preferentially resolve different environmental processes than those resolved in the open-ocean record (e.g. Immenhauser et al., 2002).

Other possible explanations for the observed relationship between $\delta^{13}C$ and sedimentation in Alpine foreland include: 1) local fluctuations in relative sea-level through subsidence variations across the Alpine foreland, or 2) tectonic uplift and denudation in the Corsica-Sardinia hinterland forcing regression in the Alpine foreland. These interpretations cannot be ruled out with the existing dataset, however the observed link between $\delta^{13}C$, eustatic highstands and sedimentation is consistent with depositional patterns observed elsewhere, making this interpretation favoured with the current data.

The sensitivity of the $\delta^{13}C$ record to various environmental forcings that can all affect deep-marine deposition is therefore a limitation as well as a strength, particularly for disentangling onshore climate and hydrological change from sea-level change. For example, warming and sea-level rise may reduce the supply of ^{12}C to deep-water by driving rivers landward, but cooling may also reduce the supply of ^{12}C to deep-water by increasing aridity, even if sea-levels are lowered. In order to fully constrain the controls on submarine fan deposition within the Alpine foreland, and other deep-marine settings, a multi-proxy approach is therefore required. In the Alpine foreland, for example, the hypothesis of eustatic control could be tested by greater constraint of hinterland uplift-subsidence patterns across the EOT, or from a detailed investigation of pollen and spore assemblages across the EOT. When

correlating data to published isotopic or sea-level curves, it is also suggested that comparisons are made between curves from different sources and derived from different methods (e.g. Miller et al., 2008; Miller et al., 2020), as processing differences between these sources can profoundly affect interpretations of paleoenvironmental change and associated uncertainties (Fig. 4).

6. Conclusion

Submarine fan evolution is intimately linked to tectonic and climatic processes. The stratigraphic record of submarine fans is therefore expected to archive major tectonic and climatic events. Here we show that positive $\delta^{13}C$ excursions correspond to periods of reduced sediment delivery to the Alpine foreland basin. These positive $\delta^{13}C$ excursions are linked to periods of eustatic highstand in the early Oligocene that decreased sediment supply to deep-water environments. Expansion of vegetation during these warmer periods may have also acted to reduce sediment supply to deep-water. Sea-level lowstands driven by icesheet expansion resulted in increased sediment supply to submarine fans and coarse-grained deposition in the basin. While alternative interpretations cannot be ruled out, this study indicates that the coupled influence of sea-level and onshore climate change across the EOT and during the early Oligocene affected submarine fan deposition in Alpine foreland, further highlighting the utility of exhumed submarine fans as archives of environmental change. Future work should seek to collect other climate-sensitive proxies, such as pollen, to further test this hypothesis.

Declaration of Competing Interest

The authors declare that they have no known competing financial interests or personal relationships that could have appeared to influence the work reported in this paper.

Acknowledgements

Soutter is funded by NERC grant number NE/M00578X/1. We thank two anonymous reviewers, Cai Puigdefàbregas, Brian Romans and Miguel Garces for their detailed comments and suggestions, which greatly improved the manuscript. We wish to thank Julie Dougans (SUERC) for technical assistance in the stable isotope analyses.

Appendix A. Supplementary data

Supplementary data to this article can be found online at https://doi.org/10.1016/j.palaeo.2022.111064.

References

Armstrong McKay, D.I., Tyrrell, T., Wilson, P.A., 2016. Global carbon cycle perturbation across the Eocene-Oligocene climate transition. Paleoceanography 31 (2), 311–329.
Beerling, D.J., Royer, D.L., 2011. Convergent cenozoic CO_2 history. Nat. Geosci. 4, 418–420.
Berggren, W.A., Kent, D.V., Swisher, C.C., Aubry, M.-P., 1995. In: Berggren, W.A., Kent, D.V., Hardenbol, J. (Eds.), Geochronology, Time Scales and Global Stratigraphic Correlations: A Unified Temporal Framework for an Historical Geology. SEPM, pp. 129–212.
Boulesteix, K., Poyatos-Moré, M., Flint, S.S., Taylor, K.G., Hodgson, D.M., Hasiotis, S.T., 2019. Transport and deposition of mud in deep-water environments: Processes and stratigraphic implications. Sedimentology 66, 2894–2925.
Brodie, M.W., Aplin, A.C., Hart, B., Orland, I.J., Valley, J.W., Boyce, A.J., 2018. Oxygen isotope microanalysis by secondary ion mass spectrometry suggests continuous 300-million-year history of calcite cementation and dolomitization in the Devonian Bakken Formation. J. Sediment. Res. 88, 91–104.
Callec, Y., 2004. The turbidite fill of the Annot sub-basin (SE France): a sequence-stratigraphy approach. Geolog. Soc. London Spec. Publ. 221 (1), 111–135.
Cande, S.C., Kent, D.V., 1995. Revised calibration of the geomagnetic polarity timescale for the late cretaceous and Cenozoic. J. Geophys. Res. Solid Earth 100, 6093–6095.
Castelltort, S., Honegger, L., Adatte, T., Clark, J.D., Puigdefàbregas, C., Spangenberg, J. E., Dykstra, M.L., Fildani, A., 2017. Detecting eustatic and tectonic signals with carbon isotopes in deep-marine strata, Eocene Ainsa Basin, Spanish Pyrenees. Geology 45, 707–710.
Chamberlain, C.P., Mix, H.T., Mulch, A., Hren, M.T., Kent-Corson, M.L., Davis, S.J., Horton, T.W., Graham, S.A., 2012. The Cenozoic climatic and topographic evolution of the western north American Cordillera. Am. J. Sci. 312, 213–262.
Covault, J.A., Romans, B.W., Graham, S.A., Fildani, A., Hilley, G.E., 2011. Terrestrial source to deep-sea sink sediment budgets at high and low sea levels: Insights from tectonically active Southern California. Geology 39, 619–622.
Cramer, B.S., Toggweiler, J.R., Wright, J.D., Katz, M.E., Miller, K.G., 2009. Ocean overturning since the late cretaceous: Inferences from a new benthic foraminiferal isotope compilation. Paleoceanography 24.
Cullen, T.M., Collier, R.E.L., Hodgson, D.M., Gawthorpe, R., Kouli, K., Maffione, M., Kranis, H., Eliassen, G.T., 2021. Deep-water syn-rift stratigraphy as archives of Early-Mid Pleistocene palaeoenvironmental signals and controls on sediment delivery. EarthArXiv. https://doi.org/10.31223/X58892.
Du Fornel, E., Joseph, P., Desaubliaux, G., Eschard, R., Guillocheau, F., Lerat, O., Muller, C., Ravenne, C., Sztrakos, K., 2004. The southern Grès d'Annot outcrops (French Alps): an attempt at regional correlation. Geol. Soc. Lond., Spec. Publ. 221, 137–160.
Ducassou, E., Migeon, S., Mulder, T., Murat, A., Capotondi, L., Bernasconi, S.M., Mascle, J., 2009. Evolution of the Nile deep-sea turbidite system during the late Quaternary: influence of climate change on fan sedimentation. Sedimentology 56, 2061–2090.
Dumont, T., Simon-Labric, T., Authemayou, C., Heymes, T., 2011. Lateral termination of the north-directed Alpine orogeny and onset of westward escape in the Western Alpine arc: structural and sedimentary evidence from the external zone. Tectonics 30.
Eldrett, J.S., Greenwood, D.R., Harding, I.C., Huber, M., 2009. Increased seasonality through the Eocene to Oligocene transition in northern high latitudes. Nature 459, 969–973.
Euzen, T., Joseph, P., Du Fornel, E., Lesur, S., Granjeon, D., Guillocheau, F., 2004. Three-dimensional stratigraphic modelling of the Grès d'Annot system, Eocene-Oligocene, SE France. Geol. Soc. Lond., Spec. Publ. 221, 161–180.
Ferguson, R., Kane, I.A., Eggenhuisen, J., Pohl, F., Tilston, M., Spychala, Y., Brunt, R., 2020. Entangled External and Internal Controls on Submarine Fan Evolution: An Experimental Perspective: The Depositional Record.
Galy, V., France-Lanord, C., Beyssac, O., Faure, P., Kudrass, H., Palhol, F., 2007. Efficient organic carbon burial in the Bengal fan sustained by the Himalayan erosional system. Nature 450, 407–410.
Hessler, A.M., Fildani, A., 2019. Deep-sea fans: tapping into Earth's changing landscapes. J. Sediment. Res. 89, 1171–1179.
Howarth, J.D., Orpin, A.R., Kaneko, Y., et al., 2021. Calibrating the marine turbidite palaeoseismometer using the 2016 Kaikōura earthquake. Nat. Geosci. 14 (3), 161–167 (In press).
Hutchinson, D.K., Coxall, H.K., Lunt, D.J., Steinthorsdottir, M., De Boer, A.M., Baatsen, M., von der Heydt, A., Huber, M., Kennedy-Asser, A.T., Kunzmann, L., Ladant, J.B., 2021. The Eocene–Oligocene transition: a review of marine and terrestrial proxy data, models and model–data comparisons. Clim. Past v. 17, 269–315.
Immenhauser, A., Kenter, J.A., Ganssen, G., Bahamonde, J.R., Van Vliet, A., Saher, M.H., 2002. Origin and significance of isotope shifts in Pennsylvanian carbonates (Asturias, NW Spain). J. Sediment. Res. 72, 82–94.
Jenkyns, H.C., 1996. Relative Sea-level change and carbon isotopes: Data from the upper Jurassic (Oxfordian) of central and Southern Europe. Terra Nova 8, 75–85.
Joseph, P., Lomas, S.A., 2004. Deep-water sedimentation in the Alpine Foreland Basin of SE France: new perspectives on the Grès d'Annot and related systems—an introduction. Geol. Soc. Lond., Spec. Publ. 221, 1–16.
Katz, M.E., Miller, K.G., Wright, J.D., Wade, B.S., Browning, J.V., Cramer, B.S., Rosenthal, Y., 2008. Stepwise transition from the Eocene greenhouse to the Oligocene icehouse. Nat. Geosci. 1, 329.
Kennett, J.P., 1977. Cenozoic evolution of Antarctic glaciation, the circum-Antarctic Ocean, and their impact on global paleoceanography. J. Geophys. Res. 82, 3843–3860.
Ladant, J.B., Donnadieu, Y., Lefebvre, V., Dumas, C., 2014. The respective role of atmospheric carbon dioxide and orbital parameters on ice sheet evolution at the Eocene-Oligocene transition. Paleoceanography 29, 810–823.
Leeder, M.R., Harris, T., Kirkby, M.J., 1998. Sediment supply and climate change: implications for basin stratigraphy. Basin Res 10 (1), 7–18.
Liu, Z., Pagani, M., Zinniker, D., DeConto, R., Huber, M., Brinkhuis, H., Shah, S.R., Leckie, R.M., Pearson, A., 2009. Global cooling during the Eocene-Oligocene climate transition. Science 323, 1187–1190.
Marshall, J.D., 1991. Climatic and oceanographic isotopic signals from the carbonate rock record and their preservation. Geol. Mag. 129, 143–160.
Miller, K.G., Kominz, M.A., Browning, J.V., Wright, J.D., Mountain, G.S., Katz, M.E., Sugarman, P.J., Cramer, B.S., Christie-Blick, N., Pekar, S.F., 2005. The Phanerozoic record of global sea-level change. Science 310, 1293–1298.
Miller, K.G., Browning, J.V., Aubry, M.P., Wade, B.S., Katz, M.E., Kulpecz, A.A., Wright, J.D., 2008. Eocene–Oligocene global climate and sea-level changes: St. Stephens Quarry, Alabama. Geol. Soc. Am. Bull. 120, 34–53.
Miller, K.G., Browning, J.V., Schmelz, W.J., Kopp, R.E., Mountain, G.S., Wright, J.D., 2020. Cenozoic sea-level and cryospheric evolution from deep-sea geochemical and continental margin records. Sci. Adv. v. 6 p.eaaz1346.
Page, M., Licht, A., Dupont-Nivet, G., Meijer, N., Barbolini, N., Hoorn, C., Schauer, A., Huntington, K., Bajnai, D., Fiebig, J., Mulch, A., 2019. Synchronous cooling and decline in monsoonal rainfall in northeastern Tibet during the fall into the Oligocene icehouse. Geology 47, 203–206.
Pearson, P.N., Foster, G.L., Wade, B.S., 2009. Atmospheric carbon dioxide through the Eocene–Oligocene climate transition. Nature 461, 1110.

Picot, M., Marsset, T., Droz, L., Dennielou, B., Baudin, F., Hermoso, M., De Rafélis, M., Sionneau, T., Cremer, M., Laurent, D., Bez, M., 2019. Monsoon control on channel avulsions in the Late Quaternary Congo Fan. Quat. Sci. Rev. 204, 149–171.

Puigdefàbregas, C., Gjelberg, J., Vaksdal, M., 2004. The Grès d'Annot in the Annot syncline: outer basin-margin onlap and associated soft-sediment deformation. Geol. Soc. Lond., Spec. Publ. 221, 367–388.

Romans, B.W., Castelltort, S., Covault, J.A., Fildani, A., Walsh, J.P., 2016. Environmental signal propagation in sedimentary systems across timescales. Earth Sci. Rev. 153, 7–29.

Saltzman, M.R., Thomas, E., 2012. Carbon isotope stratigraphy. In: Gradstein, F., et al. (Eds.), The Geologic Time Scale: Oxford. Elsevier, UK, pp. 207–232.

Savitzky, Golay, M.J.E., 1964. Soothing and differentiation of data by simplified least squares procedures. Anal. Chem. 36, 1627–1639.

Schlanger, S.O., Premoli Silva, I., 1986. Oligocene Sea-level falls recorded in mid-Pacific atoll and archipelagic apron settings. Geology 14, 392–395.

Séranne, M., 1999. Early Oligocene stratigraphic turnover on the West Africa continental margin: a signature of the Tertiary greenhouse-to-icehouse transition? Terra Nova-Oxford 11, 135–140.

Sweet, M.L., Gaillot, G.T., Jouet, G., Rittenour, T.M., Toucanne, S., Marsset, T., Blum, M. D., 2020. Sediment routing from shelf to basin floor in the Quaternary Golo System of Eastern Corsica, France, western Mediterranean Sea. GSA Bull. 132, 1217–1234.

Voigt, S., Hilbrecht, H., 1997. Late cretaceous carbon isotope stratigraphy in Europe: correlation and relations with sea level and sediment stability. Palaeogeogr. Palaeoclimatol. Palaeoecol. 134, 39–59.

Wade, B.S., Houben, A.J., Quaijtaal, W., Schouten, S., Rosenthal, Y., Miller, K.G., Katz, M.E., Wright, J.D., Brinkhuis, H., 2012. Multiproxy record of abrupt sea-surface cooling across the Eocene-Oligocene transition in the Gulf of Mexico. Geology 40 (2), 159–162.

Westerhold, T., Marwan, N., Drury, A.J., Liebrand, D., Agnini, C., Anagnostou, E., Barnet, J.S., Bohaty, S.M., De Vleeschouwer, D., Florindo, F., Frederichs, T., 2020. An astronomically dated record of Earth's climate and its predictability over the last 66 million years. Science 369, 1383–1387.

Yancey, T.E., Elsik, W.C., Sancay, R.H., Prothero, D.R., Ivany, L.C., Nesbitt, E.A., 2003. The Palynological Record of Late Eocene Climate Change, Northwest Gulf of Mexico: From Greenhouse to Icehouse-the Marine Eocene-Oligocene Transition, pp. 252–268.